Renewable Energy and Power Quality Journal
https://repqj.com/index.php/repqj/index
RE&PQJ, Vol. 23, No. 1, 2025

Projection Method for Non-Iterative Decentralized Optimal Power Flow for Multi-Area Electricity System Considering the Uncertainty of PV Power

Huafeng Liu[1], Chenhao Dai[1], Jinqiang Lin[1,*], Chenxi Dong[2], Dandan Zhai[1], Jiachen Kang[1], Hongyi Peng[3]

[1]State Grid Hubei Electric Power Co., Ltd. Xiangyang Power Supply Branch, Xiangyang, Hubei, China
[2]State Grid Hubei Electric Power Co. Ltd, Wuhan, Hubei, China
[3]Hubei Keneng Power Electronics Co. Ltd, Wuhan, Hubei, China
[*]Corresponding author's email: 2453931565@qq.com

Abstract. In this paper, a decentralized optimization method based on projection is proposed for multi-area interconnected electricity systems to enhance computational efficiency and privacy preservation. To address the challenges posed by photovoltaic (PV) uncertainty, a PV uncertainty model is proposed and translated into a certainty centralized operation model. The certainty centralized operation model decomposed into subproblems for each area. To preserve privacy, the proposed projection method transforms the operational constraints of each subproblem into a projection space that retains all essential information from the original space. This transformation conceals private variables of each area, preserving the privacy of local systems. The projection space of each subproblem constitutes the reformulated convex hull of the system, enabling the derivation of coupling variable solutions for the interconnected system. By solving the reformulated optimization problem, the coupling variables are obtained and used to decompose the problem into subproblems for each area. Each subproblem is then solved independently, avoiding iterations. This method addresses several drawbacks of traditional iterative decentralized methods, such as excessive iterations, long computation times, and potential non-convergence. Additionally, inter-area power transfer facilitates and enhances the absorption of PV generation, achieving 0 MW solar curtailment, lowering operating costs, and alleviating the impact of PV uncertainty. The effectiveness of the proposed method is verified through case studies on a 6-6 bused system and a 118-145 buses system. Results demonstrate the proposed method's ability to achieve lower computational costs, higher accuracy, and better privacy preservation compared to conventional methods. The computational time of the proposed projection method in 118-145 buses system is 0.1046 *s*, significantly shorter than the 0.2130 *s* required by the conventional centralized operational method. The findings confirm that the proposed method is a practical and efficient solution for optimizing multi-area interconnected electricity systems under PV uncertainty.

Key words. Multi-Area Electricity System, Decentralized Optimal Power Flow, PV Output Uncertainty, Projection Method, Non-Iterative Method.

Nomenclature

Indices and Sets

v, i, j	Indices of PV generator, coal-fired generators, and electric loads
b, l	Indices of electric buses and transmission lines
a	Indices of areas
s_l , e_l	The start and end bus, respectively
n	The amount of area in multi-area electricity system

Parameters

η^B	The cost per unit of load shedding
η^V	The cost per unit of curtailing PV output
$b_{0,a,i}$, $b_{1,a,i}$, $b_{2,a,i}$	The quadratic function coefficient of the operational cost of conventional generators
$PG_{a,i}^{\min}$, $PG_{a,i}^{\max}$	The minimum and maximum electricity output of conventional generator i in area a, respectively
$PL_{a,l}^{\max}$	The maximum electricity flow in electric line l in area a
$PV_{a,v,t}$	The forecast output of PV generator v at period t in area a
$PB_{a,j,t}$	The electric load j at period t in area a
$RU_{a,i}$, $RD_{a,i}$	Upward and downward ramp rates of conventional generator i in area a, respectively
$\boldsymbol{A}_a$	The parameter vectors in the objective
$\boldsymbol{B}_1$, $\boldsymbol{B}_2$, $\boldsymbol{B}_3$, …, $\boldsymbol{B}_{2n}$	The corresponding parameter matrices
$\boldsymbol{C}_1$, $\boldsymbol{C}_2$, …, $\boldsymbol{C}_{2n}$	The parameter vectors in constraints

$\Delta PV_{a,v,t}$	The output deviation of PV generator v from the forecast value at period t in area a
$KG_{a,i}$	The balance factor of conventional generator i in area a, which is a constant related to the capacity of the conventional generator
$\Delta \boldsymbol{PV}_a$	Vector of the output deviation of PV generator from the forecast value in area a
$\Delta \boldsymbol{PV}_a^{\max}$, $\Delta \boldsymbol{PV}_a^{\min}$	Vectors of the maximum and minimum of the output deviation of PV generator from the forecast value in area a, respectively
$y_a^{\max}$	The value customed by the actual situation, which is to avoid unbounded operation space after rewriting

Variables

$LS_{a,j,t}^{B}$	The load shedding of electric load j at period t in area a
$LS_{a,v,t}^{V}$	The solar curtailment of PV generators v at period t in area a
$PG_{a,i,t}$	Electricity output of conventional generators i at period t in area a
$PL_{a,l,t}$	The electricity flow of electric line l at period t in area a
$\boldsymbol{\alpha}_a$	Private variables' vector in area a
χ	The public variables' vector between different areas
$\Delta PG_{a,i,t}$	The deviation electric output of conventional generator i at period t in area a owing to the PV output deviation from forecast value
$\Delta LS_{a,j,t}^{B}$	The deviation load shedding of load j at period t in area a owing to the PV output deviation from forecast value
$\Delta LS_{a,v,t}^{V}$	The deviation solar curtailment of PV generator v at period t in area a owing to the PV output deviation from forecast value
$\boldsymbol{V}_{s,r_a}^{a}$	The vertex matrix that constitutes the boundary face s of the convex hull in the r_a -th iteration
$\boldsymbol{\lambda}_{s,r_a}^{a}$	The outward normal vector of the boundary face s of the convex hull in the r_a -th iteration

1. Introduction

Energy is the driving force behind economic and social development, and its exploration and utilization have significantly advanced social productivity and human civilization [1-3]. However, the traditional energy system, heavily dependent on fossil fuels, has led to global energy resource shortages [4,5]. At the same time, large-scale greenhouse gas emissions have exacerbated global warming, causing frequent extreme weather events [6]. To alleviate the increasing environmental pressures, there is an urgent need to develop new energy technologies characterized by green, low-carbon solutions, promoting the transition of energy towards cleaner and more sustainable forms [7]. The development of renewable energy generation technologies, particularly solar power, is one of the key strategies for replacing traditional coal-fired power generation [8-10]. In recent years, with the maturation of new energy technologies, the integration capacity of renewable energy has rapidly increased due to its diverse operation modes and relatively low generation costs [11]. According to the National Energy Administration of China, in 2023, the newly installed solar power capacity reached 609.49 million kW, a 55.2% increase year-on-year [12]. Relying on renewable energy for power generation is an effective solution to mitigate energy shortages. However, renewable energy generation faces significant uncertainties [13]. For example, solar power generation is strongly correlated with solar irradiance, which fluctuates, and the current prediction accuracy for photovoltaic (PV) generation is only around 85% [14]. These uncertainties significantly impact the scheduling of electricity systems.

With the acceleration of economic globalization and urbanization, traditional single-area electricity systems have increasingly exposed issues such as supply-demand imbalances and energy security risks [15]. As pointed out in the Case Study of [16], the generator may not supply all the load due to the transmission capacity limits and load shedding thus occurs when a single-area electricity system operates independently, resulting in energy security risks. The multi-area interconnected electricity system is defined as an electricity system managed by multiple different operators. In addition, The topological grid area managed by the same operator is defined as a single area. Interconnection of cross-area electricity systems helps fully utilize area resources and achieve supply-demand balance [17]. Therefore, the multi-area interconnected electricity systems emerged. Through cross-area electricity exchanges, surplus power from resource-rich areas can be transported to areas with high demand, ensuring effective resource allocation and utilization [18].

Therefore, this paper models and solves the optimal power flow problem in multi-area interconnected electricity systems considering the uncertainty in PV generation. The PV uncertainty is determined by the prediction accuracy, and it is still impossible to predict completely accurately [19,20]. There has been much research on the multi-area electricity system and the PV uncertainty. [21-23] explored the coordinated scheduling problem of multi-area electricity system, and proposed decentralized optimization method to enhance operational flexibility in multi-area electricity system further. Reddy, et al. [24] established the electricity system considering PV uncertainty, assuming the uncertainty in solar irradiance to follow a lognormal distribution. Wang, et al. [25] used stochastic dynamic programming to consider PV uncertainty in DC-powered renewable energy sources. Iris, et al. [26] assumed that uncertainty is represented by a set of scenarios and each scenario includes a different PV generation for each period. We consider PV uncertainty by a robust optimization method in this paper, as in [27].

Due to technical limitations (such as the high computational demands of large-scale joint solving) and regulatory concerns (such as management independence and privacy), centralized optimization methods that require global information to compute the optimal power flow in multi-area interconnected systems are impractical [28]. Therefore, decentralized optimization methods are necessary. To date, a considerable number of decentralized optimization methods have been proposed. [29-31] used the alternating direction method of multipliers (ADMM) to solve the optimal power flow problem. They introduced differentially private consensus, machine-learning approach, and single-loop structure, to improve ADMM performance. [32-34] exploited the benders-decomposition approach to enhance the mathematical tractability of the problem, enabling robust planning of renewable energy systems. Huang et al. [35] used the optimality conditioned composition (OCD) algorithm to solve the coordinated scheduling problem of integrated energy system. Previous study [36-38] introduced a two-stage programming on the basis of resilience oriented model to reinforce the resilience of power system against severe events.

However, the above-decentralized optimization method requires iterative solving, which may result in excessive iterations, long computation time, and non-iteration. Therefore, it is necessary to improve the problems caused by the iteration of decentralized optimization methods. Pan, et al. [39] proposed learning-based nearly non-iterative stochastic dynamic transactive energy control of networked microgrids, and avoid iterative. However, it does not consider privacy-preserving and limits scalability. Chen, et al. [40] proposed non-iterative multi-area coordinated energy for hybrid AC/DC power systems. However, it still needs to solve large-scale joint optimization problems.

In conclusion, among the extant methods, the centralized optimization methods exhibit flaws in privacy-preserving. The conventional decentralized optimization methods address the issue of privacy-preserving. However, they are beset with problems arising from iterations. And the non-iterative methods demand large-scale joint solution. Therefore, we proposed projection-based decentralized optimization method for multi-area electricity system. The proposed projection method addresses several drawbacks of traditional iterative decentralized methods, provides privacy-preserving, and avoid the problem of large-scale joint solution. The major contributions of this paper are shown as follows:

1) A novel projection-based decentralized optimization method is introduced to multi-area electricity system. The proposed method conceals the private variables, thus preserving the privacy of each subarea.

2) The proposed projection method reduces the variables and mitigates the complexity of the model of multi-area electricity system considering PV uncertainty.

3) The proposed projection method achieves high accuracy. Additionally, it avoids iterative and possible problems of iteration are solved, such as excessive iterations, long computation time, and non-iteration.

Additionally, section II introduces the centralized operation model considering the uncertainty of PV output. Section III introduces the procedure of projection method. Section IV designs case studies to verify the advantages of the proposed projection method. Section V concludes the paper.

2. Multi-Area Electricity System Model

A. Deterministic Operation Model

In this section, a deterministic model of the centralized operation model for multi-area electricity system is proposed.

The objective of the deterministic operation model is to minimize conventional generators' operational costs, load shedding costs, and solar curtailment costs. The objective function can be formulated as follows:

$$min\left(\sum_{a}\sum_{t}\sum_{i}C_{a,i,t}+\eta^{B}\sum_{a}\sum_{t}\sum_{j}LS^{B}_{a,j,t}+\eta^{V}\sum_{a}\sum_{t}\sum_{v}LS^{V}_{a,v,t}\right) \tag{1}$$

The cost of a single conventional generator can be formulated as follows:

$$C_{a,i,t}=b_{0,a,i}+b_{1,a,i}PG_{a,i,t}+b_{2,a,i}(PG_{a,i,t})^{2}\ \ \forall a,\forall i,\forall t \tag{2}$$

The electricity output of the conventional generators is constrained by:

$$PG^{min}_{a,i}\le PG_{a,i,t}\le PG^{max}_{a,i}\ \ \forall a,\forall i,\forall t \tag{3}$$

The electricity flow in electric lines is constrained by:

$$-PL^{max}_{a,l}\le PL_{a,l,t}\le PL^{max}_{a,l}\ \ \forall a\ ,\forall l\ ,\forall t \tag{4}$$

The electricity balance at buses is as follows:

$$\sum_{i\in b}PG_{a,i,t}+\sum_{w\in b}\left(PV_{a,v,t}-LS^{V}_{a,v,t}\right)-\sum_{j\in b}\left(PB_{a,j,t}-LS^{B}_{a,j,t}\right)=\sum_{l|s=b}PL_{a,l,t}-\sum_{l|e=b}PL_{a,l,t}\ \ \forall a\ \forall b\ \forall t \tag{5}$$

The ramping limit is as follows:

$$-RD_{a,i}\cdot\Delta t\le PG_{a,i,t+1}-PG_{a,i,t}\le RU_{a,i}\cdot\Delta t\ \ \forall a,\forall i,\forall t \tag{6}$$

The coupling constraint is as follows:

$$PL_{\Phi(s_l),l,t}=PL_{\Phi(e_l),l,t}\ \ \forall l,\forall t \tag{7}$$

where, $\Phi(\cdot)$ denotes the owning area of the bus.

The above deterministic operation model can be rewritten as:

$$
\begin{aligned}
&min\sum_{a=1}^{n} \boldsymbol{A}_a \cdot \boldsymbol{\alpha}_a \\
&\boldsymbol{B}_1 \cdot \boldsymbol{\alpha}_1 + \boldsymbol{B}_2 \cdot \boldsymbol{\chi} \le \boldsymbol{C}_1 \\
&\boldsymbol{B}_3 \cdot \boldsymbol{\alpha}_2 + \boldsymbol{B}_4 \cdot \boldsymbol{\chi} \le \boldsymbol{C}_2 \\
&\cdots \\
&\boldsymbol{B}_{2n-1} \cdot \boldsymbol{\alpha}_n + \boldsymbol{B}_{2n} \cdot \boldsymbol{\chi} \le \boldsymbol{C}_n
\end{aligned} \tag{8}
$$

B. Centralized Operation Model Considering the Uncertainty of PV Output

In this section, we introduce uncertainty information into the model proposed in the previous section. The objective function of the centralized operation model will be rewritten as follows while considering the PV output:

$$
\begin{aligned}
&\max_{\Delta PV_{a,v,t}} \min \left\{ \begin{array}{l} \sum_a \sum_t \sum_i \left[b_{0,a,i} + b_{1,a,i}(PG_{a,i,t} + \Delta PG_{a,i,t}) + \right. \\ \left. b_{2,a,i}(PG_{a,i,t} + \Delta PG_{a,i,t})^2 \right] + \\ \eta^B \sum_a \sum_t \sum_j \left(LS^B_{a,j,t} + \Delta LS^B_{a,j,t} \right) + \\ \eta^V \sum_a \sum_t \sum_v \left(LS^V_{a,v,t} + \Delta LS^V_{a,v,t} \right) \end{array} \right. \\
&\forall \Delta PV_{a,v,t} \in \left[\Delta PV^{\min}_{a,v}, \Delta PV^{\max}_{a,v} \right]
\end{aligned} \tag{9}
$$

The deviation electric output of conventional generators is as follows:

$$
\Delta PG_{a,i,t} = -KG_{a,i} \sum_v \Delta PV_{a,v,t} \quad \forall a, \forall i, \forall t \tag{10}
$$

Replace the $PV_{a,v,t}$ and $PG_{a,i,t}$ in constraints (2)-(7) as $(PV_{a,v,t} + \Delta PV_{a,v,t})$ and $(PG_{a,i,t} + \Delta PG_{a,i,t})$, respectively. In addition, other variables are also replaced with their corresponding deviation values, such as $PL_{a,l,t}$ replaced by $(PL_{a,l,t} + \Delta PL_{a,l,t})$, etc.

Refer to equation (8), the centralized operation model considering the uncertainty of PV output can be rewritten as:

$$
\begin{aligned}
&\max_{\Delta \boldsymbol{PV}} \min \sum_{a=1}^{n} \boldsymbol{A}_n \cdot \boldsymbol{\alpha}_n + \sum_{a=1}^{n} \boldsymbol{A}_{n+a} \cdot \Delta \boldsymbol{PV}_a \\
&\boldsymbol{B}_1 \cdot \boldsymbol{\alpha}_1 + \boldsymbol{B}_2 \cdot \boldsymbol{\chi} + \boldsymbol{B}_{2n+1} \cdot \Delta \boldsymbol{PV}_1 \le \boldsymbol{C}_1 \\
&\boldsymbol{B}_3 \cdot \boldsymbol{\alpha}_2 + \boldsymbol{B}_4 \cdot \boldsymbol{\chi} + \boldsymbol{B}_{2n+2} \cdot \Delta \boldsymbol{PV}_2 \le \boldsymbol{C}_2 \\
&\cdots \\
&\boldsymbol{B}_{2n-1} \cdot \boldsymbol{\alpha}_n + \boldsymbol{B}_{2n} \cdot \boldsymbol{\chi} + \boldsymbol{B}_{3n} \cdot \Delta \boldsymbol{PV}_n \le \boldsymbol{C}_n \\
&\forall \Delta \boldsymbol{PV}_a \in \left[\Delta \boldsymbol{PV}_a^{\min}, \Delta \boldsymbol{PV}_a^{\max} \right]
\end{aligned} \tag{11}
$$

where, $\boldsymbol{B}_{2n+1} \cdot \Delta \boldsymbol{PV}_1$, $\boldsymbol{B}_{2n+2} \cdot \Delta \boldsymbol{PV}_2$, $\cdots$, and $\boldsymbol{B}_{3n} \cdot \Delta \boldsymbol{PV}_n$ denote the deviation of other variables owing to the PV output deviation from forecast value.

3. Optimal Power Flow Based on Projection

A. Reformulation of the Operation Model

In this section, we reformulate the operation model to use the projection method later in the paper. Transform model (11) equivalent to (12):

$$
\begin{aligned}
&\min \sum_{a=1}^{n} \boldsymbol{A}_a \cdot \boldsymbol{\alpha}_a + \sum_{a=1}^{n} A_{n+a} \cdot \Delta \boldsymbol{PV}_a^{\min} \\
&\boldsymbol{B}_1 \cdot \boldsymbol{\alpha}_1 + \boldsymbol{B}_2 \cdot \boldsymbol{\chi} \le \boldsymbol{C}_1 - \boldsymbol{B}^+_{2n+1} \cdot \Delta \boldsymbol{PV}_1^{\max} - \boldsymbol{B}^-_{2n+1} \cdot \Delta \boldsymbol{PV}_1^{\min} \\
&\boldsymbol{B}_3 \cdot \boldsymbol{\alpha}_2 + \boldsymbol{B}_4 \cdot \boldsymbol{\chi} \le \boldsymbol{C}_2 - \boldsymbol{B}^+_{2n+2} \cdot \Delta \boldsymbol{PV}_2^{\max} - \boldsymbol{B}^-_{2n+2} \cdot \Delta \boldsymbol{PV}_2^{\min} \\
&\boldsymbol{L} \\
&\boldsymbol{B}_{2n-1} \cdot \boldsymbol{\alpha}_n + \boldsymbol{B}_{2n} \cdot \boldsymbol{\chi} \le \boldsymbol{C}_n - \boldsymbol{B}^+_{3n} \cdot \Delta \boldsymbol{PV}_n^{\max} - \boldsymbol{B}^-_{3n} \cdot \Delta \boldsymbol{PV}_n^{\min}
\end{aligned} \tag{12}
$$

The variables satisfy:

$$
\begin{aligned}
&\boldsymbol{B}^+_{2n+1} = \max\{\boldsymbol{B}_{2n+1}, 0\}, \boldsymbol{B}^-_{2n+1} = \min\{\boldsymbol{B}_{2n+1}, 0\} \\
&\boldsymbol{B}^+_{2n+2} = \max\{\boldsymbol{B}_{2n+2}, 0\}, \boldsymbol{B}^-_{2n+2} = \min\{\boldsymbol{B}_{2n+2}, 0\} \\
&\cdots \\
&\boldsymbol{B}^+_{3n} = \max\{\boldsymbol{B}_{3n}, 0\}, \boldsymbol{B}^-_{3n} = \min\{\boldsymbol{B}_{3n}, 0\}
\end{aligned} \tag{13}
$$

At this stage, uncertainty model (11) is transformed into deterministic model (13), which contains the uncertainty information of PV output.

B. The Procedure of Projection Method

In this section, we introduce the procedure of projection method, including decomposition of the centralized operation model, initialization of the vertices set, searching of more vertices, reformulation of the convex hull (the convex hull of a set of points is defined as the smallest convex set containing all points), reformulation of the optimization problem, and solution of the reformulated optimization problem, as shown in Figure 1. All areas do not directly communicate with each other. The operator of each sub-area provides public information to the centralized operator. If the relevant agency has specific transparency requirements for certain parameters, this parameter can be defined as a public variable and passed to the centralized operator, while other privacy variables remain unchanged. The centralized operator makes a unified calculation and then delivers the calculation results separately. In this procedure, the private variables are concealed, the model complexity is greatly reduced, and the projection space (the projection space is defined as the low-dimensional subspace onto which the original high-dimensional optimization problem is mapped) is completely equivalent to the operation space of the original optimization problem, ensuring the accuracy of the solution. The proof of equivalence is presented in Appendix A.

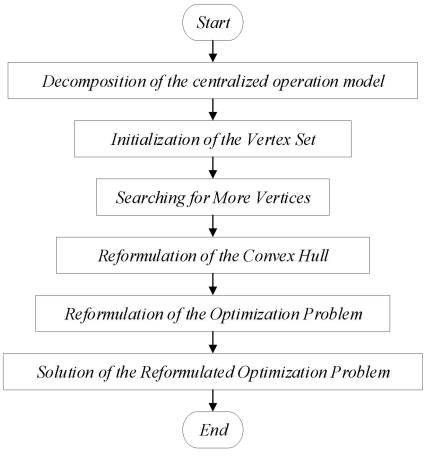

Figure 1. The procedure of projection method

1) Decomposition of the Centralized Operation Model

The centralized operational model (12) needs to be decomposed into the decentralized operation model of each subarea. Taking Area 1 as an example, the decentralized operation model is expressed as:

$$\begin{gathered}\min \boldsymbol{A}_1 \cdot \boldsymbol{\alpha}_1+\boldsymbol{A}_{\boldsymbol{n}+1} \cdot \Delta \boldsymbol{P} \boldsymbol{V}_1^{\min } \\ \boldsymbol{B}_1 \cdot \boldsymbol{\alpha}_1+\boldsymbol{B}_2 \cdot \boldsymbol{\chi} \leq \boldsymbol{C}_1-\boldsymbol{B}_{2 \boldsymbol{n}+1}^{+} \cdot \Delta \boldsymbol{P} \boldsymbol{V}^{\max }-\boldsymbol{B}_{2 \boldsymbol{n}+1}^{-} \cdot \Delta \boldsymbol{P} \boldsymbol{V}^{\min } \\ \boldsymbol{B}_{2 \boldsymbol{n}+1}^{+}=\max \left\{\boldsymbol{B}_{2 \boldsymbol{n}+1}, 0\right\}, \boldsymbol{B}_{2 \boldsymbol{n}+1}^{-}=\min \left\{\boldsymbol{B}_{2 \boldsymbol{n}+1}, 0\right\}\end{gathered} \tag{14}$$

To hide the private variable in the objective function, define a new public variable and rewrite the decentralized operation model of Area 1 as follows:

$$\begin{gathered}\min y_1 \\ \boldsymbol{B}_1 \cdot \boldsymbol{\alpha}_1+\boldsymbol{B}_2 \cdot \boldsymbol{\chi} \leq \boldsymbol{C}_1-\boldsymbol{B}_{2 \boldsymbol{n}+1}^{+} \cdot \Delta \boldsymbol{P} \boldsymbol{V}^{\max }-\boldsymbol{B}_{2 \boldsymbol{n}+1}^{-} \cdot \Delta \boldsymbol{P} \boldsymbol{V}^{\min } \\ \boldsymbol{B}_{2 \boldsymbol{n}+1}^{+}=\max \left\{\boldsymbol{B}_{2 \boldsymbol{n}+1}, 0\right\}, \boldsymbol{B}_{2 \boldsymbol{n}+1}^{-}=\min \left\{\boldsymbol{B}_{2 \boldsymbol{n}+1}, 0\right\} \\ y_1 \geq \boldsymbol{A}_1 \cdot \boldsymbol{\alpha}_1+\boldsymbol{A}_{\boldsymbol{n}+1} \cdot \Delta \boldsymbol{P} \boldsymbol{V}_1^{\min } \\ y_1 \leq y_1^{\max }\end{gathered} \tag{15}$$

2) Initialization of the Vertex Set

a) The projection space is determined by the interconnection of each subarea and the need for privacy-preserving:

In order to preserve privacy, it is necessary to hide private variables of each subarea. Taking Area 1 as an example, the public variables $\boldsymbol{\chi}$ and y_1 are selected to build the projection space, the same applies to other subareas.

b) Set Γ_a^{init} as empty.

c) Select a public variable(e.g., y_a).

d) Assign appropriate initial values $\boldsymbol{\chi}^{init}$ to variables $\boldsymbol{\chi}$ other than the variable mentioned in *c)*, these initial values must lie within their respective feasible domains.

e) In conjunction with the conditions of d), determine the maximum and minimum values of the selected variables in *c)*, which can be formulated as the following problem (taking subarea 1 as an example):

$$\begin{gathered}\max (\min) \ y_1 \\ \boldsymbol{B}_1 \cdot \boldsymbol{\alpha}_1+\boldsymbol{B}_2 \cdot \boldsymbol{\chi}^{init} \leq \boldsymbol{C}_1-\boldsymbol{B}_{2 \boldsymbol{n}+1}^{+} \cdot \Delta \boldsymbol{P} \boldsymbol{V}^{\max }-\boldsymbol{B}_{2 \boldsymbol{n}+1}^{-} \cdot \Delta \boldsymbol{P} \boldsymbol{V}^{\min } \\ \boldsymbol{B}_{2 \boldsymbol{n}+1}^{+}=\max \left\{\boldsymbol{B}_{2 \boldsymbol{n}+1}, 0\right\}, \boldsymbol{B}_{2 \boldsymbol{n}+1}^{-}=\min \left\{\boldsymbol{B}_{2 \boldsymbol{n}+1}, 0\right\} \\ y_1 \geq \boldsymbol{A}_1 \cdot \boldsymbol{\alpha}_1+\boldsymbol{A}_{\boldsymbol{n}+1} \cdot \Delta \boldsymbol{P} \boldsymbol{V}_1^{\min } \\ y_1 \leq y_1^{\max }\end{gathered} \tag{16}$$

Solve problem (16), get the result $y_1^{\max}$ and $y_1^{\min}$. Define two vertices as $\left[y_1^{\max},(\boldsymbol{\chi}^{init})^{\boldsymbol{T}}\right]$ and $\left[y_1^{\min},(\boldsymbol{\chi}^{init})^{\boldsymbol{T}}\right]$, and add them to the initial vertex set Γ_a^{init} .

f) Repeat c)-e) for other public variables, such as variables in vector $\boldsymbol{\chi}$, to obtain the complete initial vertex set of Area *a*. The amount of vertices in the initial vertex set is denoted as N_0 .

g) The coordinate origin is shifted to the interior of the convex hull formed by the initial vertex set, in order to facilitate the subsequent computation of outward normal vectors at the boundaries:

$$\begin{gathered}\boldsymbol{v}_i^a=\boldsymbol{v}_i^a-\boldsymbol{v}_{avg}^a \ \ \forall i=1, \cdots, N_0 \\ \boldsymbol{v}_{avg}^a=\frac{1}{N_0} \sum_{i=1}^{N_0} \boldsymbol{v}_i^a\end{gathered} \tag{17}$$

3) Searching for More Vertices

a) Set $r_a=0$, and set Γ_a^{ver} to Γ_a^{init} .

b) $r_a=r_a+1$.

c) Solve to obtain the convex hull constituted by the vertex set Γ_a^{ver} .

d) Individually compute the outward normal vector corresponding to each boundary face of the convex hull in c):

$$\boldsymbol{V}_{s, r_a}^a \boldsymbol{\lambda}_{s, r_a}^a=1 \tag{18}$$

When the coordinate origin is located inside the convex hull, the outward normal vector can be solved using (18).

e) For each boundary face *s*, search outward along its outward normal vector λ_{s,r_a}^a to find the farthest vertex by solving (19) under the constraints of model (15).

$$\begin{gathered}\boldsymbol{v}^a=\left[y_a, \boldsymbol{\chi}^{\boldsymbol{T}}\right] \\ v_{s, r_a}^{a *}=\underset{v^a}{argmax}\left(I_{s, r_a}^a=\left(v^a-v_{avg}^a\right) \cdot \lambda_{s, r_a}^a\right)\end{gathered} \tag{19}$$

Denote the I_{s,r_a}^{a*} value corresponding to v_{s,r_a}^{a*} as I_{s,r_a}^{a*}

f) I_{s,r_a}^{a*} satisfying (20) indicates a new vertex has been found, and add the corresponding vertex v_{s,r_a}^{a*} to vertex set Γ_a^{ver} .

$$er_{s, r_a}^a=I_{s, r_a}^{a *}-1>\varepsilon_1 \tag{20}$$

Where, ε_1 is a small positive constant.

g) Repeat b)-f). No new vertices outside the required precision range remain when (21) is satisfied, and the loop terminates.

$$\max_{s} er_{s,r_a}^{a} \le \varepsilon_2 \tag{21}$$

Where, ε_2 denotes the remaining residual.

4) Reformulation of the Convex Hull

a) Solve to obtain the convex hull constituted by the vertex set Γ_a^{ver}.

b) Individually compute the outward normal vector corresponding to each boundary face of the convex hull in a):

$$\boldsymbol{V}_s^a \boldsymbol{\lambda}_s^a = 1 \tag{22}$$

where, $\boldsymbol{V}_s^a$ is the vertex matrix that constitutes the boundary face s of the convex hull. $\boldsymbol{\lambda}_s^a$ denotes the outward normal vector of the boundary face s of the convex hull.

c) The constraints of the projected operation space for the subproblem are as follows:

$$\begin{aligned} \boldsymbol{v}^a &= [y_a, \boldsymbol{\chi}^T] \\ \left(\boldsymbol{v}^a - \boldsymbol{v}_{avg}^a\right) \cdot \boldsymbol{\lambda}_s^a &\le 1 \ \forall s \end{aligned} \tag{23}$$

At this point, private variables have been hidden, and the constraints in the projected operation space only contain the public variables, privacy of each area is effectively protected.

d) Each subarea provides the information obtained in *c)* to the centralized operator.

5) Reformulation of the Optimization Problem

The centralized operator combines the projected constraints of each subproblem into the reconstructed convex hull (25), and derives the reconstructed optimization problem (24)-(25).

$$\min \sum_{a} y_a \tag{24}$$

$$\begin{aligned} \boldsymbol{v}^a &= [y_a, \boldsymbol{\chi}^T] \ \forall a \\ \left(\boldsymbol{v}^a - \boldsymbol{v}_{avg}^a\right) \cdot \boldsymbol{\lambda}_s^a &\le 1 \ \forall s \ \forall a \end{aligned} \tag{25}$$

The reconstructed optimization problem (24)-(25) obtained by the centralized operator contains only public variables, effectively preserving the privacy of each subarea. Furthermore, the reconstructed optimization problem (24)-(26) is fully equivalent to model (12). It retains the optimality information of the original model. By solving the reconstructed optimization problem (24)-(25), the centralized operators can obtain the values of the public variables y_a and $\boldsymbol{\chi}$, denoted as y_a^* and $\boldsymbol{\chi}^*$.

6) Solution of the Reformulated Optimization Problem

The centralized operator returns the obtained $\boldsymbol{\chi}^*$ to each subarea operator. Each subarea operator substitutes $\boldsymbol{\chi}^*$ into their respective subproblems (14) to form the reconstructed subproblem. After substitution, each subproblem can be solved independently. Each subarea operator can obtain the optimal power flow for their area.

4. Case Study

We illustrated the validity of the projection method through the demonstration of two multi-area electricity system, namely the 6-6 buses system and the 118-145 buses system.

All of the experiments were performed on a personal computer using a MATLAB R2024b platform in Gurobi 11.0.3 with Intel(R) Core(TM) i7-14700F CPU(2.10 GHz) and 32 GB of memory.

A. 6-6 Buses System

6-6 buses system consists of 2 areas. It is an improved version of standard models. Area 1 has 6 buses, 4 conventional generators, 1 PV generator, 7 transmission lines, and 2 loads. Area 2 has 6 buses, 3 conventional generators, 1 PV generator, 11 transmission lines, and 2 loads. Bus 5 in Area 1 is connected to Bus 3 in Area 2 via a tie line, as shown in Figure 2. Two systems are designed to illustrate the advantages of the multi-area interconnected electricity system:

MAS-I: Each area operates independently, with no energy flow between areas.

MAS-II: Multi-area electricity system operate interconnectedly, energy is translated between areas through transmission lines.

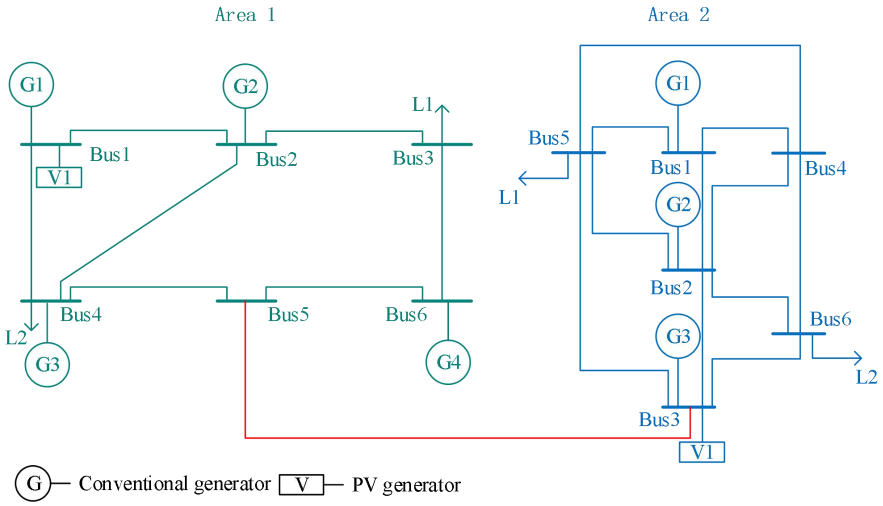

Figure 2. The topology of the 6-6 buses system

Table 1 compares two cases. Where, the total cost is the objective function (1). In MAS-I, a solar curtailment of 3.3338 MW occurs in Area 1 to maintain electricity balance. Additionally, total cost including cost of conventional generators and solar curtailment is 3.6607*104 $. In MAS-II, with multi-area electricity system operating interconnectedly, the PV output in Area 1 is absorbed by Area 2, resulting in 0 MW solar curtailment in both areas and a tie-line flow of 46.2439 MW. Additionally, the total cost of MAS-II is lower than MAS-I. Conventional generation costs in MAS-II are also lower, as the solar curtailment in MAS-I forces the conventional generators to increase output, raising their operational costs. Thus, interconnection improves PV absorption and reduces system operation costs.

Table 1. Comparison of different system

Case	Total solar curtailment (MW)		Tie-line flow at t=1(Area 1 to Area 2, MW)	Cost of conventional generators ($)	Cost of solar curtailment ($)	Total cost ($)
	Area 1	Area 2				
MAS-I	3.3338	0	0	$3.3273*10^4$	$3.3338*10^3$	$3.6607*10^4$
MAS-II	0	0	46.2439	$3.2324*10^4$	0	$3.2324*10^4$

Two cases are designed to verify the validity of projection method.

Case A: Solved the multi-area electricity system by centralized operational method.

Case B: Solved the multi-area electricity system by projection method.

We compare the results of Case A and B in 6-6 buses system, as shown in Table 2-Table 4. The convex hull after projection is exactly equivalent to the operation space of the original optimization problem in the projection method procedure (when $\varepsilon_2 = 0$ as shown in (21)). Therefore, the two methods should also be the same. When the remaining residual ε_2 is set to 0.1, although the public variables obtained by the two methods are slightly different (as shown in Table 4), the optimal cost and optimal conventional generator output solved through both methods are almost consistent (as shown in Table 2-Table 3). The calculation error formula is defined as the deviation in total cost results between the projection method and the centralized operational method: $e = (F - F_0)/F_0$. Where, F denotes the total cost results calculated by the projection method. F_0 denotes the total cost results calculated by the centralized operational method. The calculation error of the projection method in MAS-II is 0.09%. The accuracy of projection in Case B has been effectively verified.

Table 2. Comparison of the cost calculated in 6-6 buses system of different cases

Case	Cost ($)		
	Area 1	Area 2	Total cost
A	$2.0480*10^4$	$1.1844*10^4$	$3.2324*10^4$
B	$2.0459*10^4$	$1.1869*10^5$	$3.2327*10^4$

Table 3. Comparison of conventional generator output calculated in 6-6 buses system of different cases

Case		Output of conventional generator (MW)			
		t=1	t=2	t=3	t=4
A	G3	24.6468	21.1972	17.7542	21.6207
	G4	20.4408	22.4113	24.3901	25.8307
B	G3	24.6468	21.1972	17.7542	21.6207
	G4	20.4408	22.4113	24.3901	25.8307

Table 4. Comparison of tie-line flow calculated in 6-6 buses system of different cases

Case	Tie-line flow (MW)			
	t=1	t=2	t=3	t=4
A	46.2375	26.3157	5.1797	27.2091
B	42.3942	24.7516	4.3934	31.4074

B. 118-145 Buses System

118-145 buses system consists of 2 areas. It is an improved version of standard models. Area 1 has 118 buses, 54 conventional generators, 18 PV generators, 186 transmission lines, and 99 loads. Area 2 has 145 buses, 50 conventional generators, 14 PV generators, 453 transmission lines, and 60 loads. Bus 3 in Area 1 is connected to Bus 1 in Area 2 via a tie line.

The PV forecasting error is defined as the maximum possible ratio of deviation from the forecasted output of PV generators. We adjusted the PV forecasting error values and obtained the evolution of total cost with respect to the forecasting error, as shown in Figure 3. As the PV forecasting error increases, the total cost under forecasted output also increases. When the actual PV output deviates significantly from the forecasted value, conventional generators need to balance the system while maintaining sufficient margin. It leads to operation at suboptimal cost levels relative to the forecasted output. Therefore, the total cost increases. The larger the PV forecasting error the higher total costs.

We compare the number of variables of variables and constraints, computational time, and the solved total cost in 118-145 buses system of different cases to verify the advantages of projection method, as shown in Table 5. Projection method only adopts public variables rather than all public and private variables to solve the multi-area electricity system. Therefore, the number of variables in Case B is significantly reduced compared with that in Case A. The privacy of each area is preserved and the complexity of the model is reduced. Additionally, the number of constraints in Case B is increased compared with that in Case A, which leads to a tight operation space and thus reduces the computational time. Meanwhile, the total cost of the two cases is equivalent. The reduced variable count stems directly from the dimensionality reduction process. The increased constraints are an inherent consequence of equivalently representing the original high-dimensional problem in the low-dimensional space. The privacy preservation, low complexity, fast calculation, and high accuracy of projection method are verified.

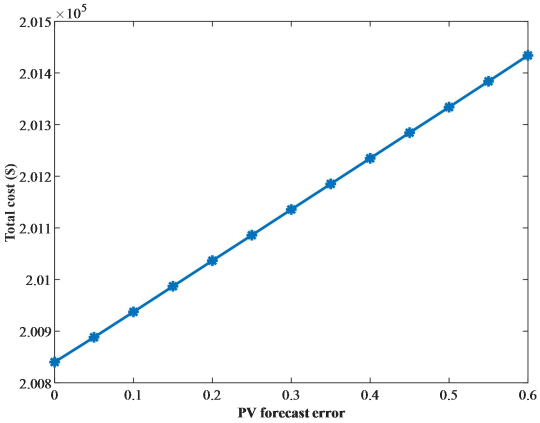

Figure 3. Evolution of the total cost as a function of the PV power forecasting error in 118-145 buses system

Table 5. Comparison of the number of variables and constraints, computational time, and the solved total cost in 118-145 buses system of different cases

Case	Number of variables	Number of constraints	Computational time (s)	Total cost ($)
A	16260	84	0.2130	$2.0104*10^5$
B	5	422	0.1046	$2.0104*10^5$

5. Conclusion

This paper is to propose a projection method for non-iterative decentralized optimal power flow for multi-area electricity system considering the uncertainty of PV power. The proposed projection method includes the following procedure: decomposition of the centralized operation model, initialization of the vertices set, searching of more vertices, reformulation of the convex hull, reformulation of the optimization problem, and solution of the reformulated optimization problem. The private variables of each subarea are concealed in this procedure. The centralized operator uses only public variables to solve the optimal power flow problem of multi-area electricity system. Therefore, the projection method preserves the privacy of each subarea. Additionally, the projection method has the advantages of low complexity, fast calculation, and high accuracy. We verify those advantages in 6-6 buses electricity system and 118-145 buses electricity system in the case study. Moreover, we design several cases to introduce the advantage of multi-area electricity system operating interconnectedly, and the impact of PV output uncertainty on system cost.

When the proposed projection method is applied to large systems with thousands of buses, it may increase the number of public variables if the interconnected area increases. Therefore, the dimensions of the projected convex hull increase accordingly. It will increase the searching time of the vertex set. We plan to explore more efficient convex hull vertex search methods in future research to solve this problem.

The projection method is designed for optimization-based scheduling problems. Thus, evolving PV forecasting techniques directly leads to more optimal scheduling solutions. Additionally, the proposed projection method can be adapted to other renewable energy sources like wind or hybrid systems, and to other types of renewable energy uncertainties. It only requires modifying the original mathematical model and applying the same projection method as presented in this work. While current experiments focus on simulations, we plan to pursue real-world testing given future deployment opportunities. In practical applications, the proposed projection method can also be integrated with machine learning-based uncertainty forecasting.

Acknowledgements

This paper was funded by State grid xiangyang electricity co.Ltd 2024 distributed photovoltaic scale perception and risk analysis application development project, Grant Number 7415D0240005.

References

[1] S.P. Li, J. Meng, H.R. Zheng, N. Zhang, J.W. Huo, et al. The driving forces behind the change in energy consumption in developing countries. Environmental Research Letters, 2021, 16(5), 054002. DOI: 10.1088/1748-9326/abde05

[2] X. Zhao, D.K. Luo. Driving force of rising renewable energy in China: Environment, regulation and employment. Renewable and Sustainable Energy Reviews, 2017, 68(4), 48-56. DOI: 10.1016/j.rser.2016.09.126

[3] P. Sadorsky. Wind energy for sustainable development: Driving factors and future outlook. Journal of Cleaner Production, 2021, 289, 125779. DOI: 10.1016/j.jclepro.2020.125779

[4] W.S. Ebhota, T.C Jen. Fossil fuels environmental challenges and the role of solar photovoltaic technology advances in fast tracking hybrid renewable energy system. International Journal of Precision Engineering and Manufacturing-Green Technology, 2019, 7(4), 97-117. DOI: 10.1007/s40684-019-00101-9

[5] Y.L. Zhukovskiy, D.E. Batueva, A.D. Buldysko, B. Gil, V.V. Starshaia. Fossil energy in the framework of sustainable development: analysis of prospects and development of forecast scenarios. Energies, 2021, 14(17), 5268. DOI: 10.3390/en14175268

[6] X.Z. Tan, X.X. Wu, Z.Q. Huang, J.Y. Fu, X.J. Tan, et al. Increasing global precipitation whiplash due to anthropogenic greenhouse gas emissions. Nature Communications, 2023, 14(1), 2796. DOI: 10.1038/s41467-023-38510-9

[7] K.S. Woon, Z.X. Phuang, J. Taler, P.S. Varbanov, C.T. Chong, et al. Recent advances in urban green energy development towards carbon emissions neutrality. Energy, 2023, 267, 126502. DOI: 10.1016/j.energy.2022.126502

[8] L.X. Yao, Z.W. Guan, Y. Wang, H.X. Hui, S.Y. Luo, et al. Evaluating the feasibility of concentrated solar power as a replacement for coal-fired power in China: A comprehensive comparative analysis. Applied Energy, 2025, 377, 124396. DOI: 10.1016/j.apenergy.2024.124396

[9] Y. Shuai, E. Shagdar, B.G. Lougou, A. Mustafa, B. Doljinsuren, et al. Performance analysis of 200 MW solar coal hybrid power generation system for transitioning to a low carbon energy future. Applied Thermal Engineering, 2021, 183, 116140. DOI: 10.1016/j.applthermaleng.2020.116140

[10] S.S. Gharehveran, K. Shirini, S.C. Khavar, S.H. Mousavi, A. Abdolahi. Deep learning-based demand response for short-term operation of renewable-based microgrids. The Journal of Supercomputing, 2024, 80(18), 26002-26035. DOI: 10.1007/s11227-024-06407-z

[11] E. Erdiwansyah, M.A. Taleb, H. Husin, N. Syafie, M.S. Zaki, et al. A critical review of the integration of renewable energy sources with various technologies. Protection and Control of Modern Power Systems, 2021, 6(1), 3. DOI: 10.1186/s41601-021-00181-3

[12] 2023 national power industry statistics. National Energy Administration, 2024.

[13] M.M.R. Ahmed, S. Mirsaeidi, M.A. Koondhar, N. Karami, E.M. Tag-Eldin, et al. Mitigating Uncertainty Problems of Renewable Energy Resources Through Efficient Integration of Hybrid Solar PV/Wind Systems Into Power Networks. IEEE Access, 2024, 12, 30311-30328. DOI: 10.1109/ACCESS.2024.3370163

[14] R. Ahmed, V. Sreeram, Y. Mishra, M.D. Arif. A review and evaluation of the state-of-the-art in PV solar power forecasting: Techniques and optimization. Renewable and Sustainable Energy Reviews, 2020, 124, 109792. DOI: 10.1016/j.rser.2020.109792

[15] A.J. Conejo, J.A. Aguado. Multi-area coordinated decentralized DC optimal power flow. IEEE

Transactions on Power Systems, 1998, 13(4), 1272-1278. DOI: 10.1109/59.736264
[16] M.Y. Yan, X.M. Ai, J.Y. Wen, Y.B. He, Y.N. Zhang. Decentralized optimization for multi-area optimal transmission switching via iterative ADMM. 2018 IEEE Power & Energy Society General Meeting (PESGM), 2018, 1-5. DOI: 10.1109/PESGM.2018.8586669
[17] W.T. Lu, M.B. Liu, S.J. Lin, L.C. Li. Fully decentralized optimal power flow of multi-area interconnected power systems based on distributed interior point method. IEEE Transactions on Power Systems, 2017, 33(1), 901-910. DOI: 10.1109/TPWRS.2017.2694860
[18] J.Q. Zhu, X.M. Mo, Y.R. Xia, Y. Guo, J.J. Chen, et al. Fully-decentralized optimal power flow of multi-area power systems based on parallel dual dynamic programming. IEEE Transactions on Power Systems, 2021, 37(2), 927-941. DOI: 10.1109/TPWRS.2021.3098812
[19] K. Shirini, M.B. Kordan, S.S. Gharehveran. Impact of learning rate and epochs on lstm model performance: a study of chlorophyll-a concentrations in the Marmara Sea. The Journal of Supercomputing, 2025, 81(1), 1-18. DOI: 10.1007/s11227-024-06806-2
[20] Y. Gheibi, K. Shirini, S.N. Razavi, M. Farhoudi, T. Samad-Soltani. CNN-Res: deep learning framework for segmentation of acute ischemic stroke lesions on multimodal MRI images. BMC Medical Informatics and Decision Making, 2023, 23(1), 192. DOI: 10.1186/s12911-023-02289-y
[21] H. Zhang, X. Hu, H.Z. Cheng, S.Z. Zhang, S.Y. Hong, et al. Coordinated scheduling of generators and tie lines in multi-area power systems under wind energy uncertainty. Energy, 2021, 222, 119929. DOI: 10.1016/j.energy.2021.119929
[22] W. Gan, M.Y. Yan, W. Yao, J.B. Guo, X.M. Ai, et al. Decentralized computation method for robust operation of multi-area joint regional-district integrated energy systems with uncertain wind power. Applied Energy, 2021, 298(1), 117280. DOI: 10.1016/j.apenergy.2021.117280
[23] X.M. Dong, Y. Ma, Y. Wang, Q. Chen, Z.Q. Liu, et al. An improved power flow calculation method based on linear regression for multi-area networks with information barriers. International Journal of Electrical Power & Energy Systems, 2022, 142, 108385. DOI: 10.1016/j.ijepes.2022.108385
[24] Y. Reddy, J. Jithendranath, A.K. Chakraborty, J.M. Guerrero. Stochastic optimal power flow in islanded DC microgrids with correlated load and solar PV uncertainties. Applied Energy, 2022, 307(1), 118090. DOI: 10.1016/j.apenergy.2021.118090
[25] X.L. Wang, Q.S. Hua, P. Liu, L. Sun. Stochastic dynamic programming based optimal energy scheduling for a hybrid fuel cell/PV/battery system under uncertainty. Process Safety and Environmental Protection, 2022, 165, 380-386. DOI: 10.1016/j.psep.2022.07.025
[26] Ç. Iris, J.S.L. Lam. Optimal energy management and operations planning in seaports with smart grid while harnessing renewable energy under uncertainty. Omega, 2021, 103(3), 102445. DOI: 10.1016/j.omega.2021.102445
[27] M.Y. Yan, W. Gan, Y. Zhou, J.F. Wen, W. Yao, et al. Projection method for blockchain-enabled non-iterative decentralized management in integrated natural gas-electric systems and its application in digital twin modelling. Applied Energy, 2022, 311(3), 118645. DOI: 10.1016/j.apenergy.2022.118645
[28] H.Y. Peng, M.Y. Yan, Y.J. Zhou. Privacy-preserving non-iterative decentralized optimal energy flow for integrated hydrogen-electricity-heat system based on projection method. Applied Energy, 2024, 368, 123470. DOI: 10.1016/j.apenergy.2024.123470
[29] C. Lei, S.Q. Bu, Q.F. Chen, Q.G. Wang, Q. Wang, et al. Decentralized Optimal Power Flow for Multi-Agent Active Distribution Networks: A Differentially Private Consensus ADMM Algorithm. IEEE Transactions on Smart Grid, 2024, 15(6), 6175-6178. DOI: 10.1109/TSG.2024.3451793
[30] T.W.K. Mak, M. Chatzos, M. Tanneau, P.V. Hentenryck. Learning regionally decentralized ac optimal power flows with admm. IEEE Transactions on Smart Grid, 2023, 14(6), 4863-4876. DOI: 10.1109/TSG.2023.3251292
[31] S. Kiani, K. Sheshyekani, H. Dagdougui. ADMM-based hierarchical single-loop framework for EV charging scheduling considering power flow constraints. IEEE Transactions on Transportation Electrification, 2023, 10(1), 1089-1100. DOI: 10.1109/TTE.2023.3269050
[32] S. Daniar, F. Aminifar, H. Lesani. Optimal controlled-islanding with AC power flow constraints: A benders-decomposition approach. Electric Power Systems Research, 2023, 216(5), 108970. DOI: 10.1016/j.epsr.2022.108970
[33] F. García-Muñoz, S. Dávila, F. Quezada. A benders decomposition approach for solving a two-stage local energy market problem under uncertainty. Applied Energy, 2023, 329, 120226. DOI: 10.1016/j.apenergy.2022.120226
[34] L. Göke, F. Schmidt, M. Kendziorski. Stabilized Benders decomposition for energy planning under climate uncertainty. European Journal of Operational Research, 2024, 316(1), 183-199. DOI: 10.1016/j.ejor.2024.01.016
[35] J.B. Huang, Z.G. Li, Q.H. Wu. Coordinated dispatch of electric power and district heating networks: A decentralized solution using optimality condition decomposition. Applied Energy, 2017, 206, 1508-1522. DOI: 10.1016/j.apenergy.2017.09.112
[36] S.S. Gharehveran, S. Ghassemzadeh, N. Rostami. Two-stage resilience-constrained planning of coupled multi-energy microgrids in the presence of battery energy storages. Sustainable Cities and Society, 2022, 83, 103952. DOI: 10.1016/j.scs.2022.103952
[37] M. Ahrari, K. Shirini, S.S. Gharehveran, M.G. Ahsaee, S. Haidari, et al. A security-constrained robust optimization for energy management of active distribution networks with presence of energy storage and demand flexibility. Journal of Energy Storage, 2024, 84(7), 111024. DOI: 10.1016/j.est.2024.111024
[38] S.S. Gharehveran, S.G. Zadeh, N. Rostami. Resilience-oriented planning and pre-positioning of vehicle-mounted energy storage facilities in community microgrids. Journal of Energy Storage, 2023, 72(22), 108263. DOI: 10.1016/j.est.2023.108263
[39] Z.N. Pan, T. Yu, J. Li, Y.F. Wu, J.B. Chen, et al. Multi-agent learning-based nearly non-iterative stochastic dynamic transactive energy control of networked microgrids. IEEE Transactions on Smart Grid, 2021, 13(1), 688-701. DOI: 10.1109/TSG.2021.3116598
[40] R. Chen, J. Xu, H.R. Zhang, Y.Z. Sun, S.Y. Liao, et al. Non-iterative multi-area coordinated energy and reserve allocation model for hybrid AC/DC power systems with flexible frequency operation. Energy Reports, 2023, 9(2), 1077-1085. DOI: 10.1016/j.egyr.2023.06.047

Appendix A

Renumber the formula (15) as (26), which is the subproblem of area 1:

$$\begin{gathered}\min y_1 \\ \boldsymbol{B}_1 \cdot \boldsymbol{\alpha}_1 + \boldsymbol{B}_2 \cdot \boldsymbol{\chi} \le \boldsymbol{C}_1 - \boldsymbol{B}_{2\boldsymbol{n}+1}^{+} \cdot \Delta \boldsymbol{PV}^{\max} - \boldsymbol{B}_{2\boldsymbol{n}+1}^{-} \cdot \Delta \boldsymbol{PV}^{\min} \\ \boldsymbol{B}_{2\boldsymbol{n}+1}^{+} = \max\{\boldsymbol{B}_{2\boldsymbol{n}+1}, 0\}, \boldsymbol{B}_{2\boldsymbol{n}+1}^{-} = \min\{\boldsymbol{B}_{2\boldsymbol{n}+1}, 0\} \\ y_1 \ge \boldsymbol{A}_1 \cdot \boldsymbol{\alpha}_1 + \boldsymbol{A}_{\boldsymbol{n}+1} \cdot \Delta \boldsymbol{PV}_1^{\min} \\ y_1 \le y_1^{\max} \end{gathered} \tag{26}$$

Rewrite the operation space of optimization problem (26) into a more precise mathematical form:

$$\Gamma^1 = \left\{ (y_1, \boldsymbol{\alpha}_1, \boldsymbol{\chi}) \left| \begin{array}{c} \boldsymbol{B}_1 \cdot \boldsymbol{\alpha}_1 + \boldsymbol{B}_2 \cdot \boldsymbol{\chi} \le \boldsymbol{C}_1 - \boldsymbol{B}_{2\boldsymbol{n}+1}^{+} \cdot \Delta \boldsymbol{PV}^{\max} - \boldsymbol{B}_{2\boldsymbol{n}+1}^{-} \cdot \Delta \boldsymbol{PV}^{\min} \\ \boldsymbol{B}_{2\boldsymbol{n}+1}^{+} = \max\{\boldsymbol{B}_{2\boldsymbol{n}+1}, 0\}, \boldsymbol{B}_{2\boldsymbol{n}+1}^{-} = \min\{\boldsymbol{B}_{2\boldsymbol{n}+1}, 0\} \\ y_1 \ge \boldsymbol{A}_1 \cdot \boldsymbol{\alpha}_1 + \boldsymbol{A}_{\boldsymbol{n}+1} \cdot \Delta \boldsymbol{PV}_1^{\min} \\ y_1 \le y_1^{\max} \end{array} \right. \right\} \tag{27}$$

By merely employing y_1 and $\boldsymbol{\chi}$ to represent the operation space in (27), (27) can be equivalently expressed as (28):

$$\Gamma_{proj}^1 = \left\{ (y_1, \chi) \middle| \exists \boldsymbol{\alpha}_1, s.t. (y_1, \alpha_1, \chi) \in \Gamma^1 \right\} \tag{28}$$

The operation space represented by set Γ_{proj}^1 is fundamentally the intersection of multiple half-spaces. Therefore, the operation space represented by set Γ_{proj}^1 can be re-expressed using linear constraints again:

$$\begin{gathered}\min y_1 \\ s.t.\ \boldsymbol{V}^1 \cdot \boldsymbol{\Lambda}^1 \le \boldsymbol{H}^1 \end{gathered} \tag{29}$$

Combined with the actual calculation in the manuscript, (29) can be specifically written as (30):

$$\begin{gathered}\min y_1 \\ \boldsymbol{v}^1 = [y_1, \boldsymbol{\chi}^T] \\ \left(\boldsymbol{v}^1 - \boldsymbol{v}_{avg}^1\right) \cdot \boldsymbol{\lambda}_s^1 \le 1 \ \forall s \end{gathered} \tag{30}$$

Extended it to all area yields (24)-(25) in the manuscript. Based on the above derivation, the projected operation space is completely equivalent to the original operation space.